
Validation of Turbulent Flow in a Two-Stroke Grail Engine Cylinder

¹Shoeb Ahmed Syed*, ²Peter O. Oyekola

¹School of Mechanical Engineering, Papua New Guinea University of Technology
Lae, Papua New Guinea

²Department of Mechanical Engineering, Tennessee Tech University
Cookeville, TN 38505, USA

*Corresponding author Email: shoeb.syed@pnguot.ac.pg

Abstract: The validation of results obtained from a static computational fluid dynamics (CFD) simulation of a state-of-the-art hybrid two-stroke Grail internal combustion engine design to analyze the effects of the intake hole and channel shape on in-cylinder flow turbulence is presented in this research. The turbulent flow dynamics within the cylinder have a significant impact on combustion efficiency and pollution production in an internal combustion engine. Turbulent kinetic energy (TKE) is almost entirely generated during the in-take stroke in most engines. This considerably improves the mixture of fuel and air during the compression stage, resulting in better mixing. Therefore, in the current investigation, a considerable effort was made to focus on analyzing the effects of the intake hole, the duct shapes of the Grail engine on the in-cylinder flow dynamics. The analysis of the Grail Engine design flow field using Autodesk CFD software has produced promising results. A violent tornado-like effect is seen in the flow field. The swirl effect of the flow was observed with a single vortex located at the cylinder's axis. The Grail Engine's resulting flow field will provide an ideal homogeneous/stoichiometric fuel-air combination for increased combustion efficiency. The result of 3-D static simulations of the flow through the engine had provided guidelines on selection of several geometrical parameters for optimal performance. The values of velocity profiles and the velocity vector contours obtained from the numerical simulation are well within the limits obtained from the references.

Keywords: Grail Engine, Internal Combustion, Fluid Flow, Turbulence.

1. Introduction

While Internal combustion (IC) engines play a major role in the automotive industry today due to its physical size, economics as well as reliability. However, in understanding the operation parameters which affects system efficiency such as flow characteristics (turbulence in particular), theoretical experimental and practical analysis becomes imperative. However, several obstacles and challenges are associated with a thorough analysis of this factors given that turbulence is a fundamental physical condition which is critical in the enhancement of reliable and cleaner combustion engines. Because the in-cylinder flow pattern has such a large impact on the performance of IC engines, it's vital to numerically validate the flow field so that it can be compared to experimental data in order to improve and alter engine design for maximum performance.

IC engines remains significant despite the increasing popularity of electric vehicles which only accounts for an estimate of 2% of total automobile sale as well as 0.5% of global fleet [1]. While the increasing popularity of the electric automobiles have been primarily due to pollution concerns, intensive research efforts have been applied in reducing the impact of pollution caused by the IC engines in practical applications. Negative consequences such as the emission of carbon monoxide, unburnt hydrocarbons as well as nitrogen oxide which tends to be emitted from IC engines have been significantly reduced. However, there is still possibilities of further efficiency given the large amount of IC engines in service across a wide range of fields of which electronic systems cannot be substituted.

The shape, position, orientation of components such as the valve when combined with the cylinder head design will determine the flow pattern i.e., tumble or swirl within the cylinder [2, 3, 4]. This is further influenced by the injection mechanism, air-fuel mixing ratio, piston position etc. During the engine intake stroke, the valve allows high stream jets of air-fuel mix into the cylinder which generates swirls flow where

the fluid angular velocity goes around the axis of the cylinder. Tumble flow, on the other hand, follows an axis that runs parallel to the cylinder axis. Better understanding of this flow pattern has previously been investigated using steady swirl test rigs in the cylinder. This also aid in the improvement of combustion chamber design of IC engines such as homogeneous-charged compression ignition (HCCI) engines, gasoline direct injection (GDI) engines, and so on.

According to Heywood [3] experimental study, tumble and swirl vortices which are formed during the intake stroke of the engine is the factor which initiates high turbulence towards the compression stroke which in turns leads to higher combustion efficiency. Similar studies have implemented the particle image velocimetry (PIV) technique to investigate cylinder mixing pattern to estimate the angular velocity and intensity of turbulent flows in premixed charge compression ignition (PCCI) engine [4], cylinder tumble flow in IC engine operating at variable speed for the duration of the intake and compression stroke of the engine [5]. This is because the PIV methodology is a non-intrusive technique which is capable of determining multiple velocity components in both two and three dimensions.

Reynolds Averaged Navier Stokes (RANS) have also been used in analyzing and optimizing engine geometry as it provides a mean quantity of values at a relatively low computational cost. However, it is not capable of detailing information on the individual cycle as opposed to the large eddy simulation (LES), which details underlying small scales however at the expense of higher computational resources [6, 7].

There are different methods to the adaptation of the PIV technique in engine performance analysis depending on the quantity of interest for instance when analyzing a system with one exposure per cycle, then the regular low repetition rate PIV is utilized [8, 9, 10, 11, 12]. This have been used in the analyses of spatial flow structures in the characterization of turbulent properties [13, 14]. The volumetric instantaneous flow field have also been investigated using the tomographic PIV and holographic PIV in assessing the overall strain tensor and vorticity vector in the cylinder [15, 16, 17, 18, 19]. The goal of this research is to conduct a CFD simulation of the flow dynamics and turbulence efficiency of a single-cylinder two-stroke Grail engine to aid Grail Engine Technologies' ongoing design efforts. This CFD analysis involves static and dynamic mesh simulations of flow inside the intake valve and its channels to determine the best shapes for these regions to generate enough turbulent kinetic energy (TKE) within the cylinder and increase engine performance.

2. Grail Engine Technology

The Grail engine used in this study is a unique two stroke engine which features a unique configuration and design characteristics as compared to the commercially available models. As seen in the figure 1, the major components are the single intake valve which sits on the piston head, exhaust valve centralized on top of the cylinder head surrounded by three ignition sparkplugs and a single fuel injector. There are also two intake tube channels on opposing side of the piston port with intake tunes attached.

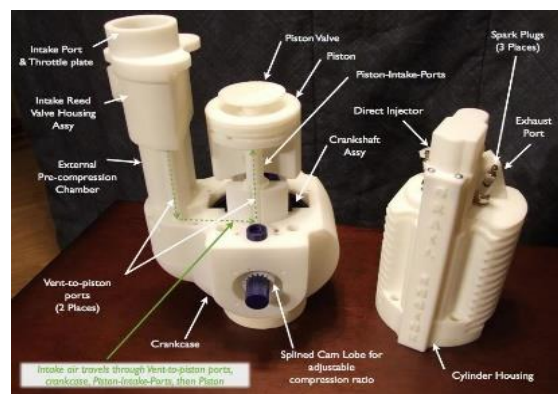


Fig. 1. Parts of Grail engine model [1]

Because of the design's uniqueness, when the piston moves upward, a vacuum is created in the tube channels, allowing fresh air to charge the tube through the one-way reed valve after fuel injection in the combustion chamber during the compression stroke. The air-fuel mixture is ignited by the three sparkplugs. The resulting explosion pushes the piston downwards, creating compression pressure in the tube channel, which forces fresh air into the combustion chamber while wasted gases are evacuated from the exhaust valve at the cylinder's top.

This cycle introduced the Grail cycle, which is a hybrid of homogeneous-charged compression ignition and forced semi-homogeneous-charged compression ignition that works in tandem with the Miller cycle (FS-HCCI). This means that in this engine architecture, there is no cross contamination of fuel and air, thereby reducing emissions while providing great power and torque with significantly less fuel than conventional IC engines. The engine is also designed to operate using multiple fuel type, variable compression ratio and thus can boast of better efficiency as well as higher mileage projection.

3. Cylinder Fluid Flow

Different flow characteristics are exhibited in the grail engine at different cycle stages. During the intake stroke, air flows inside the cylinder from the inlet valve in the form of a jet whose flow depends on the design characteristics such as geometry of the ports, location, valves, timing etc. the incoming jet fluid flow energy creates flow structures featuring large scale turbulence in the cylinder in the form of swirl flow which rotates round the cylinder's axis or tumble flow characterized by a flow pattern perpendicular to the axis of the cylinder as in figure 2. This accelerates the transport phenomenon as well as spread the air-fuel mixture within the cylinder uniformly.

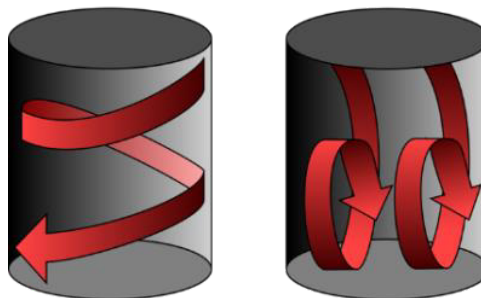


Fig. 2. Swirl and tumble flow structures [3, 19]

Most of the turbulence is further diminished due to fluid viscosity at the second phase of the intake stroke. The compression stroke of the piston increases the density which changes the turbulence length scale of the flow which increases the turbulence despite continual presence of viscous decay. This turbulence is minimal at the end of the exhaust stroke.

4. Numerical Methodology

Modelling fluid turbulence analytically is quite tasking especially when analyzing practical problems. Simulations and computer aided tools are then applied in solving the governing equations. Due to the limits of high computational needs when using the direct numerical simulation (DNS) method in IC applications, RANS and large eddy simulation (LES) have been used [20]. Typically, the mesh required in modelling the RANS model is capable of capturing up to 85-90% of the fluid global characteristics and kinetic energy [21] and was applied in this study using the Autodesk CFD simulation solver based on the standard K- ϵ model [22]. The operating conditions and specifications of the Grail engine model are listed in Table 1.

The compressible flow Navier-Stokes's equations were solved by applying the implicit segregated solver as well as the monotone streamline upwind scheme governing the in-cylinder flow.

The governing PDEs are shown below [23]-[24]:

Continuity equation: $\nabla \cdot (\rho V) = 0$ (1)

Momentum equation: $\rho(V \cdot \nabla V) = \rho g - \nabla P + (\mu + \mu_t)\nabla^2 V + S_\omega + S_{DR}$ (2)

Energy equation: $\rho C_p(V \cdot \nabla T) = (k + k_t)\nabla^2 T + q_V$ (3)

Table 1. Engine Specification for CFD Analysis

Engine Parameters	Unit	Value	Engine Parameters	Unit	Value
Cylinders	-	1	Connecting rod length	(in)	5
Engine Type	-	two-stroke	Crank radius	(in)	1.5
Displacement Volume	(in ³)	36.08644844	Compression ratio	-	15.06
Bore	(in)	3.8	Max intake valve lift	(in)	0.25
Stroke	(in)	3	Max exhaust valve lift	(in)	0.25

For driven flow, the cylinder walls had a no-slip boundary condition, and the intake and outflow pressures were 10 and 0 psig, respectively. The default simulation variables were utilized to calculate the tangential velocity component in terms of translational and rotational motion of the boundary walls, while the solid viscous surfaces were subjected to an adiabatic temperature condition and a zero-pressure gradient. A SIMPLE-R algorithm was implemented as the segregation solver and the finite element Galerkin's weighted residual method was applied on the diffusion and source terms.

5. Results and Discussions

Given that Autodesk CFD finite element solver is new to IC engine applications, such as the Grail engine, it is required to determine the solver's current applicability to an IC engine and to validate the solver using published experimental models. Accordingly, two flow validation model is considered in this paper. The work presented here is part of my PhD thesis [25]. The two validation models are shown in Figure 3.



Fig. 3. Validation model 1 and 2 geometrical details (dimensions in mm) [26, 28]

An axis-symmetric rapid expansion with a stationary valve is used in validation model 1. The downstream pipe's diameter is 3.5 times that of the upstream pipe. With a Reynolds number of 30,000, a constant mass flow rate of 0.05 kg/sec is provided at the input. The results are validated by comparing them to Grosjean et al experimental LDA measurement data [26]. The RANS flow equations are solved using the Autodesk finite element solver. These calculations are carried out on a full three-dimensional (3-D) unstructured mesh with 4.1 million components using the Autodesk standard k-ε turbulence model.

Figure 4 shows two-dimensional (2-D) mesh slices for the validation model and the boundary-layer elements near the intake valve, respectively. The mesh is grouped at the valve head, as seen, in order to properly model the vortices while limiting CPU time. Boundary-layer elements near the wall and unstructured tetrahedral elements away from the wall make up the mesh. The region around the valve is fine-tuned using three levels of Autodesk's auto-gradation mesh technology. The wall function is used to compute the distance between the wall and the stresses that occur near the wall.

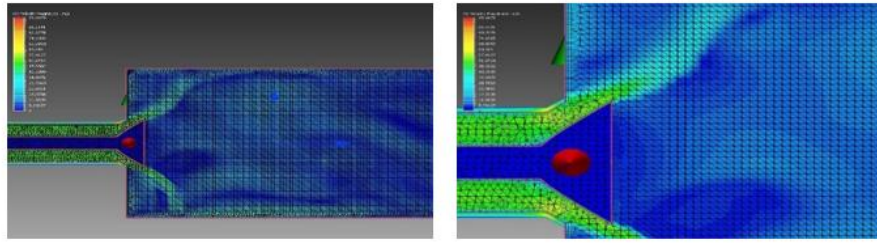


Fig. 4. 2-D slice of mesh for validation model 1

During the intake stroke of a typical IC engine, large-scale vortical fluid motion arises downstream of the intake valve. Turbulence is created by the vortical motions created during the intake stroke, which aids in greater fuel-air mixing and combustion efficiency in the later phases of the engine's operation. The effectiveness of the Autodesk CFD solver to capture these vortices in the sudden-expansion geometry is assessed using this model. Figures 5 and 6 illustrate axial mean velocity and root mean square (RMS) velocity profiles from the cylinder head at $z = 20$ mm and $z = 70$ mm, respectively. When the RANS simulation results are compared to the LDA measurements of Grosjean et al. [26], they indicate that the RANS and LDA data are in good agreement. RANS is superior at predicting the peaks of axial mean velocities at both axial sites due to valve jet breakdown. RANS simulations capture the steep peaks of fluctuations (RMS velocities) reasonably effectively.

The peaks are slightly dispersed, and the peak's position is slightly shifted. The wall model utilized in the Autodesk finite element solver is to blame for the disparity between numerical and experimental results in the region near to the cylinder wall.

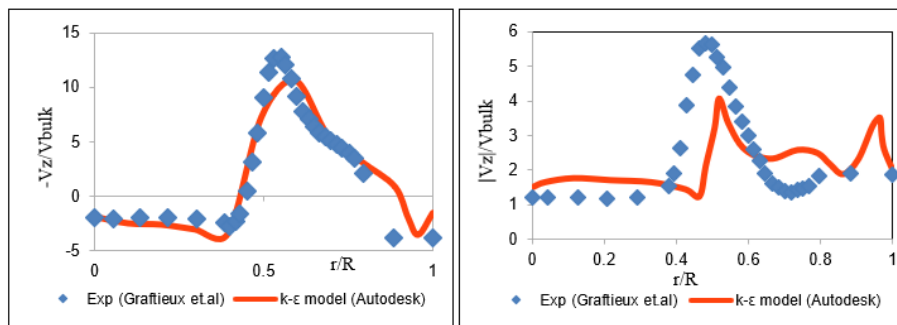


Fig. 5. Validation Model 1 Axial Velocity Profiles at $z = 20$ mm (a) Mean Axial Velocity (b) RMS Axial Velocity

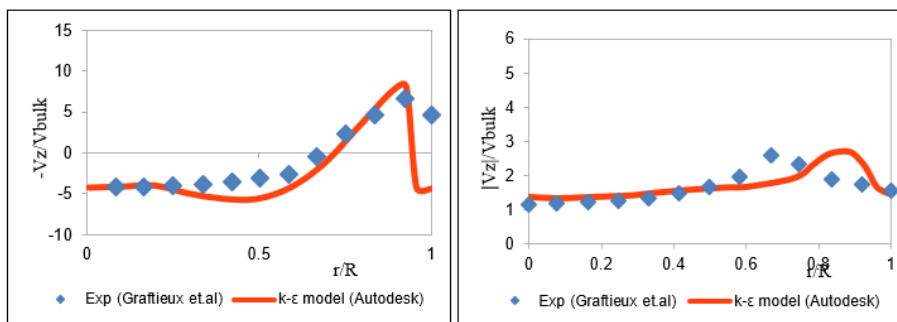


Fig. 6. Validation Model 1 Axial Velocity Profiles at $z = 70$ mm (a) Mean Axial Velocity (b) RMS Axial Velocity

The velocity vector contour plot in Figure 7(a) confirms the creation of large-scale vortical fluid motions downstream of the valve and in the cylinder head and cylinder wall corners. The accelerating fluid jet enters the cylinder and collides with the walls, splitting the flow into three zones. The wake-like flow structures are created by the vortices that develop at the corners of the cylinder near the head on either side, and the reflected section near the wall.

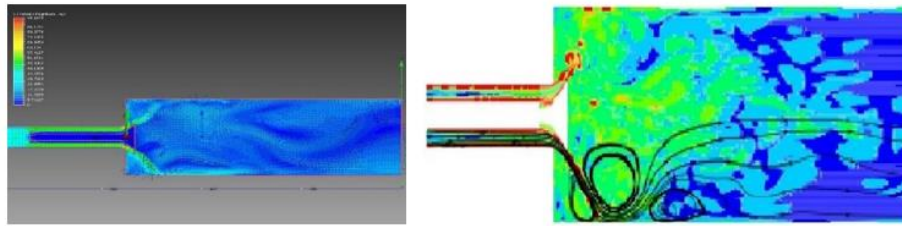


Fig. 7 (a) Validation Model Velocity vector contour-plot (b) Streamline flow structures [27]

The flow structures reported by Banaeizadeh et al. [27] are illustrated in Figure 7(b), which corresponds to the velocity vector contour plot shown in Figure 7(a) from the current simulation. Figure 8 depicts the validation model 2, which is a simple piston-cylinder arrangement with a stationary open valve. The chosen flow was ideal for deciphering in-cylinder flow dynamics and evaluating the Autodesk CFD solver technique in complex geometries with shifting boundaries and turbulence model capabilities to capture turbulence. With a low RPM of 200, the model has a stationary open valve with the piston moving in simple harmonic motion. Based on the cylinder diameter and piston action, the flow Reynolds number is 2000. The non-dimensional velocity profile in the data is plotted using the calculated mean piston velocity (V_p) of 0.4 m/sec. The experimental data was available for the numerical results to be validated. Morse et al. [28] used LDA to measure phase-averaged mean and rms radial profiles of axial velocity at 10 mm increments starting from the cylinder head for crank angles 36 deg and 144 deg after top dead center for crank angles 36 deg and 144 deg after top dead center for crank angles 36 deg and (ATDC).

Validation model 2 was simulated using a 3-D unstructured mesh with 6.6 million elements. Figures 8 illustrate 2-D mesh slices showing the clustered mesh region surrounding the valve and piston. Because the model includes a moving piston, Autodesk CFD's moving mesh techniques are used in the simulation. To perceive the interaction between a moving solid and the fluid in its path, the mesh density of the solid and the fluid in its path must be dense enough. The piston surface mesh size is 0.09, while the fluid mesh size is 0.1, yielding a mesh of 6.6 million elements. In the region of the valve and the piston, the wall function is used, resulting in a wall y^+ value of 30.

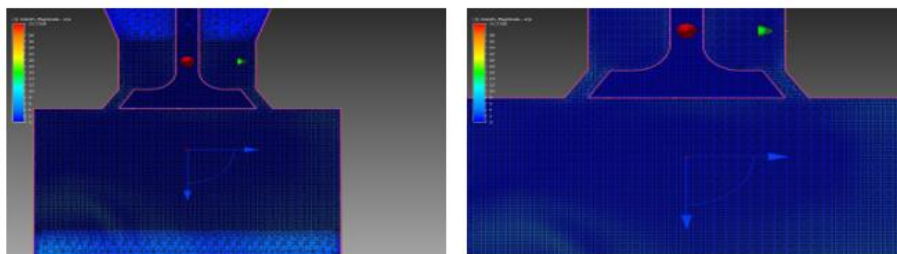


Fig. 8. Validation Model 2 2-D Slice Mesh

The governing equations are discretized using a segregated finite element solver. To solve governing equations, the RANS model is used. To provide a converged solution, a time step of 0.001 seconds was chosen with 10 internal iterations. The ideal gas model was used to model air. The advection term is discretized using the ADV1 technique, which is more numerically stable. A constant static atmospheric pressure is applied to the model's intake as a boundary condition. Solid walls are adiabatic, which means they don't slip. The piston was programmed to move in a linear motion at 200 RPM.

Figures 9–11 illustrate the comparison of numerical and experimental mean and rms radial profiles of axial velocity at 36 degrees after top dead center (TDC) at $z = 10$ mm, $z = 20$ mm, and $z = 30$ mm from the cylinder head, respectively. The numerical results are in good agreement with Morse et al experimental data [28]. The RANS model is clearly better at predicting mean profiles, as seen in the Figures. The rms profiles, on the other hand, are quite well captured by the model. Because of the more dissipative nature of the turbulence model, which tends to smooth out all velocity gradients, the peaks of rms profiles are a little flat. Figures 12 to 14 show the identical profiles as Figures 9 to 11 but with a crank angle of 144 degrees after TDC, with excellent results. At different crank angles, the profiles have the same level of agreement. One thing to keep in mind is that the flow varies significantly from cycle to cycle, and this change in velocity profiles should be considered.

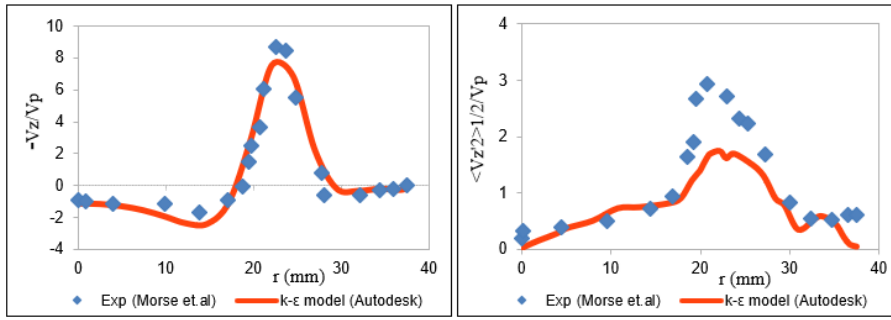


Fig. 9. Validation Model 2 Velocity Profiles for 36° CA at z = 10 mm (a) Mean Axial Velocity (b) RMS Axial Velocity

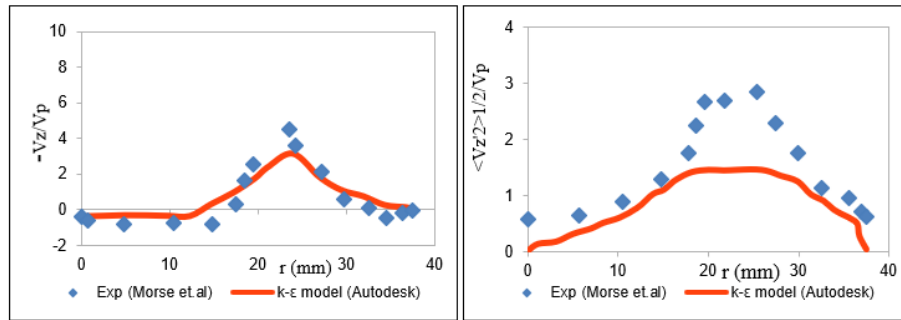


Fig. 10. Validation Model 2 Velocity Profiles for 36° CA at z = 20 mm (a) Mean Axial Velocity (b) RMS Axial Velocity

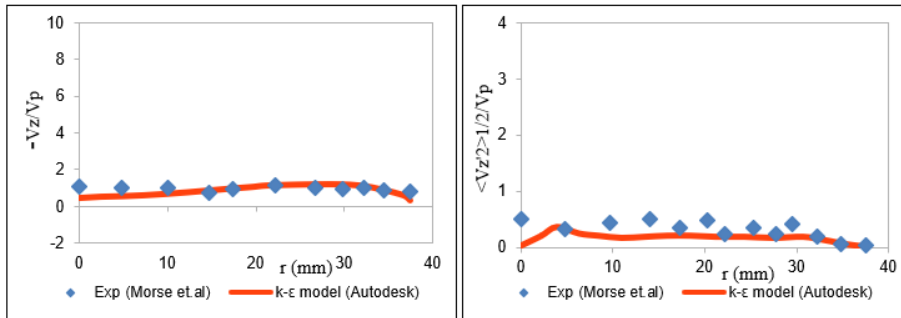


Fig. 11. Validation Model 2 Velocity Profiles for 36° CA at z = 10 mm (a) Mean Axial Velocity (b) RMS Axial Velocity

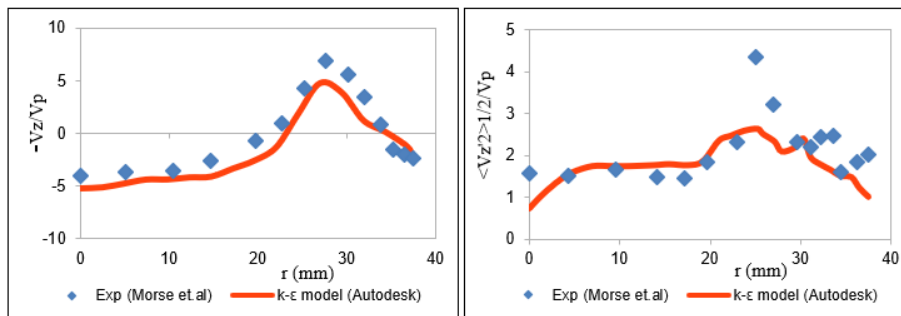


Fig. 12. Validation Model 2 Velocity Profiles for 144° CA at z = 10 mm (a) Mean Axial Velocity (b) RMS Axial Velocity

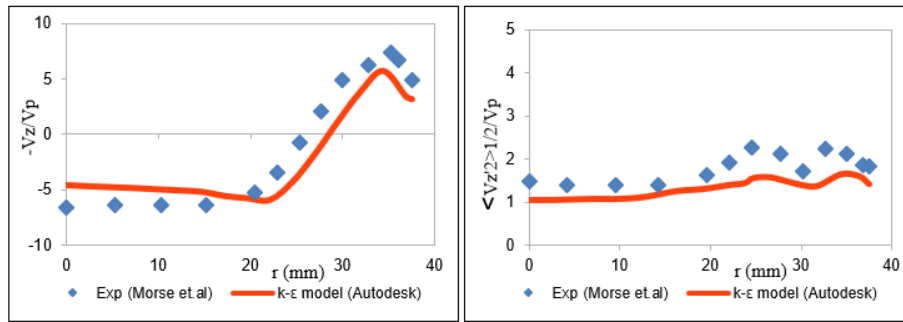


Fig. 13. Validation Model 2 Velocity Profiles for 144° CA at z = 20 mm (a) Mean Axial Velocity (b) RMS Axial Velocity

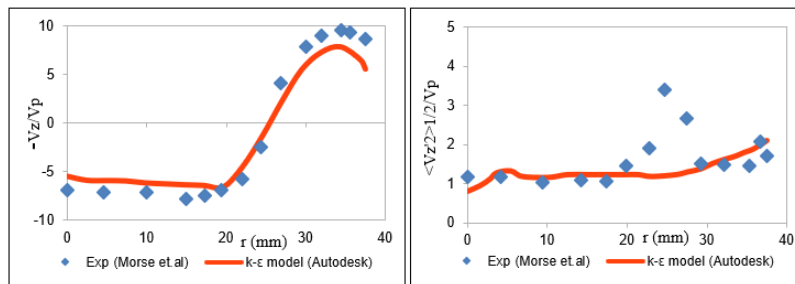


Fig. 14. Validation Model 2 Velocity Profiles for 144° CA at z = 30 mm (a) Mean Axial Velocity (b) RMS Axial Velocity

Jet enters the cylinder through the annular gap between the valve and the cylinder head as the piston descends. Due to viscous factors, this high-speed jet impinges on the side of the cylinder wall, separating the flow into vortical flow structures. The vortices, which grow in size as the piston moves down, entirely dominate the flow. Figure 16 displays velocity vector graphs obtained from the RANS model at crank angles of 90 degrees and 180 degrees, respectively, demonstrating the same behavior. Figures 16 and 17 compare these figures to the large Eddy simulation (LES) of the same model at the same crank angles performed by Verzicco et al. [29]. The flow structures in both simulations are similar, with the exception that the LES simulation has more tiny flow structures, as expected.

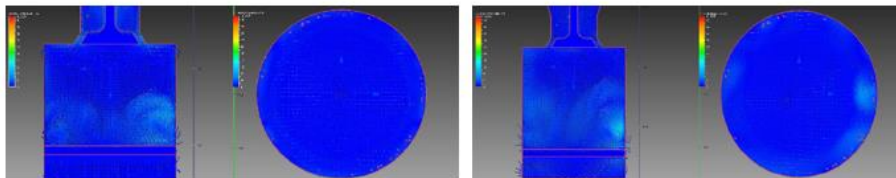


Fig. 15. Validation Model 2 RANS Velocity Vector Contour Plot at 90 and 180 degrees, respectively

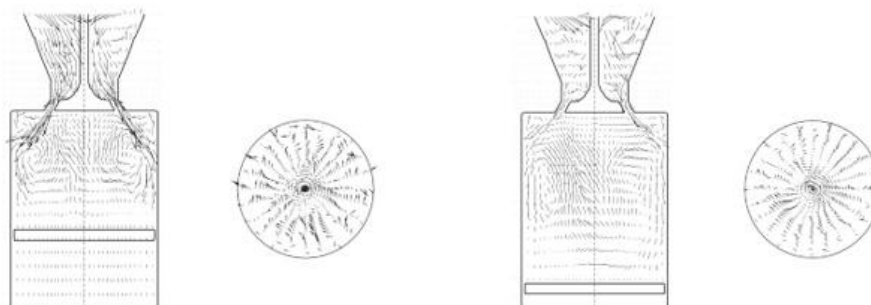


Fig. 16. Validation Model 2 LES Velocity Vector Contour Plot at 90 and 180 degrees, respectively [29]

6. Conclusion and Recommendation

This paper presents the static CFD simulation of the inflow In-cylinder flow dynamics of the Grail engine by a comparative analysis of two different model of flow which were based on flow round a fixed intake valve and a piston cylinder assembly with a top mounted fixed open valve. The result of the simulation aligns with the results obtained from experimental data. The paper focused on the initial static analysis of the Grail engine. From the CFD analysis, it was concluded that the optimal design of the piston will be a rectangular hole as well as a D-tube configuration. Furthermore, the efficiency determination criterion was based on the combination of all characteristics i.e., intake swirl flow, minimum drop in pressure in channel flow as well as an ideal mass flow rate within the cylinder.

Lastly, it is recommended in the later part of research to add in the dynamic simulation and as well as to use LES simulation model to validate the turbulent kinetic energy and the turbulence in the engine.

References

1. Global E V Outlook 2020 – Analysis - IEA. <https://www.iea.org/reports/global-ev-outlook-2020> (accessed May 15, 2021).
2. Murali Krishna, B., Bijucherian, A., Mallikarjuna, J. M.: Effect of intake manifold inclination on intake valve flow characteristics of a single cylinder engine using particle image velocimetry, World Acad. Sci. Eng. Technol. (2010).
3. Heywood, John B.: Internal Combustion Engine Fundamentals. 2nd ed. New York: McGraw-Hill Education. <https://www.accessengineeringlibrary.com/content/book/9781260116106> (2018)
4. Zegers, R.R., Meyden, V.D., Luijten, C.C., Dam, N.N., Baert, R.R., Goey, D.: Crank angle resolved flow field characterization of a Heavy-Duty (PCCI) Engine (2009)
5. Murali Krishna, B., Mallikarjuna, J. M. : Effect of engine speed on in-cylinder tumble flows in a motored internal combustion engine - An experimental investigation using particle image velocimetry, J. Appl. Fluid Mech. (2011) doi: 10.36884/jafm.4.01.11895.
6. Irannejad, A., Banaeizadeh, A., Jaber, F : Large eddy simulation of turbulent spray combustion, Combust. Flame (2015). doi: 10.1016/j.combustflame.2014.07.029.
7. Fox, R. O.: Large-eddy-simulation tools for multiphase flows, Annu. Rev. Fluid Mech. (2011) doi: 10.1146/annurev-fluid-120710-101118.
8. Lacour, C., Pera, C.: An Experimental Database Dedicated to the Study and Modelling of Cyclic Variability in Spark-Ignition Engines with LES," SAE Technical Paper 2011-01-1282 (2011) <https://doi.org/10.4271/2011-01-1282>.
9. Agarwal, A. K., Gaddekar, S, Singh, A. P.: In-cylinder air-flow characteristics of different intake port geometries using tomographic PIV," Physics of Fluids, vol. 29, no. 9, p. 095104 (2017).
10. Richard, S., Dulbecco, A., Angelberger, C., Truffin, K.: Development of a one-dimensional computational fluid dynamics modeling approach to predict cycle-to-cycle variability in spark-ignition engines based on physical understanding acquired from large-eddy simulation, Int. J. Engine Res. (2015) doi: 10.1177/1468087414560592.
11. Robert, A., Truffin, K., lafrate, N., Jay, S., Colin, O., Angelberger, C. : Large-eddy simulation analysis of knock in a direct injection spark ignition engine, Int. J. Engine Res. (2019), doi: 10.1177/1468087418796323.
12. Sofianopoulos, A., Rahimi Boldaji, M., Lawler, B, Mamalis, S.: Investigation of thermal stratification in premixed homogeneous charge compression ignition engines: A Large Eddy Simulation study, Int. J. Engine Res. (2019) doi: 10.1177/1468087418795525.
13. Bucker, I., Karhoff, D. C., Klaas, M, Schröder, W.: Stereoscopic multi-planar PIV measurements of in-cylinder tumbling flow, Exp. Fluids (2012) doi: 10.1007/s00348-012-1402-5.
14. Dannemann, J., Pielhop, K., Klaas, M., Schröder, M.: Cycle resolved multi-planar flow measurements in a four-valve combustion engine (2011) doi: 10.1007/s00348-010-0963-4.
15. Baum, E., Peterson, B., Surmann, C., Michaelis, D., Böhm, B., Dreizler, A.: Investigation of the 3D flow field in an IC engine using tomographic PIV, Proc. Combust. Inst., (2013) doi: 10.1016/j.proci.2012.06.123.
16. Peterson, B., Baum, E., Ding, C. P., Michaelis, D., Dreizler, A., Böhm, B.: Assessment and application of tomographic PIV for the spray-induced flow in an IC engine, Proc. Combust. Inst., (2017) doi: 10.1016/j.proci.2016.06.114.
17. Buchmann, N. A., Atkinson, C., Jeremy, M. C., Soria, J.: Tomographic particle image velocimetry investigation of the flow in a modeled human carotid artery bifurcation (2011) doi: 10.1007/s00348-011-1042-1.

18. Zentgraf, F., Baum, E., Böhm, B., Dreizler, A., Peterson, B.: Analysis of the turbulent in-cylinder flow in an IC engine using tomographic and planar PIV measurements, 17th Int. Symp. Appl. Laser Tech. to Fluid Mech. (2014).
19. Gadekar, S., Singh, A. P., Agarwal, A. K.: Tomographic PIV Evaluation of In-Cylinder Flow Evolution and Effect of Engine Speed (2016) doi: 10.4271/2016-01-0638.
20. Sirignano, W. A. : Volume averaging for the analysis of turbulent spray flows, Int. J. Multiph. Flow (2005), doi: 10.1016/j.ijmultiphaseflow.2005.02.005.
21. EL TAHRY S., HAWORTH, D.: Directions in turbulence modeling for in-cylinder flows in reciprocating engines (1991) doi: 10.2514/6.1991-516.
22. Launder B. E., Spalding, D. B.: The numerical computation of turbulent flows, Comput. Methods Appl. Mech. Eng. (1974) doi: 10.1016/0045-7825(74)90029-2.
23. Discretization Method | CFD | Autodesk Knowledge Network. <https://knowledge.autodesk.com/support/cfd/learn-explore/caas/CloudHelp/cloudhelp/2014/ENU/SimCFD/files/GUID-DEE0664D-771B-4446-9ED4-1498267D13FB-htm.html> (accessed Apr. 25, (2021).
24. General Fluid Flow and Heat Transfer Equations | CFD Autodesk Knowledge Network. <https://knowledge.autodesk.com/support/cfd/learn-explore/caas/CloudHelp/cloudhelp/2014/ENU/SimCFD/files/GUID-83A92AE5-0E9E-4E2D-B61F-64B3696E5F66-htm.html> (accessed Apr. 25, 2021).
25. Syed, S. A.: Numerical simulation of turbulent flow inside the cylinder of a new two-stroke grail engine design, PhD Thesis, Wichita State University (2015).
26. Grosjean, N., Graftieaux, L., Michard, M., Hübner, W., Tropea, C., Volkert, J.: Combining LDA and PIV for turbulence measurements in unsteady swirling flows, Meas. Sci. Technol. (1997), doi: 10.1088/0957-0233/8/12/015.
27. Banaeizadeh, A., Afshari, A., Schock, H., Jaber, F.: Large-eddy simulations of turbulent flows in internal combustion engines, Int. J. Heat Mass Transf. (2013) doi: 10.1016/j.ijheatmasstransfer.2012.12.065.
28. Morse, A. P., Whitelaw, J. H., Yianneskis, M.: Turbulent flow measurements by laser-doppler anemometry in motored piston-cylinder assemblies, J. Fluids Eng. Trans. ASME (1979) doi: 10.1115/1.3448937.
29. Mohd-Yusof, J., Orlandi, Paolo, Haworth, D.: LES in complex geometries using boundary body forces". Proceedings of the Summer Program (1998).